IEEE Access
Multidisciplinary | Rapid Review | Open Access Journal

SPECIAL SECTION ON EMERGING DEEP LEARNING THEORIES AND METHODS FOR BIOMEDICAL ENGINEERING

Received September 14, 2020, accepted October 14, 2020, date of publication October 29, 2020,
date of current version November 17, 2020.

Digital Object Identifier 10.1109/ACCESS.2020.3034684

Extended ResNet and Label Feature Vector Based Chromosome Classification

CHENGYU WANG[1], LIMIN YU[2], (Member, IEEE), XU ZHU[3], (Senior Member, IEEE), JIONGLONG SU[4], AND FEI MA[4]

[1]Department of Electrical Engineering and Electronics, University of Liverpool-Xi'an Jiaotong-Liverpool University, Suzhou 215123, China
[2]Department of Electrical and Electronic Engineering, Xi'an Jiaotong-Liverpool University, Suzhou 215123, China
[3]Department of Electrical Engineering and Electronics, University of Liverpool, Liverpool L69 7ZX, U.K.
[4]Department of Mathematical Sciences, Xi'an Jiaotong-Liverpool University, Suzhou 215123, China

Corresponding author: Fei Ma (fei.ma@xjtlu.edu.cn)

This work was supported in part by the National Natural Science Foundation of China (Grant No. 61501380), the QingLan project of Jiangsu Province, Laboratory of Computational Physics under Grant 6142A05180501, Xi'an Jiaotong-Liverpool University (XJTLU) Research Development Fund RDF-17-02-51, XJTLU research enhancement fund REF-19-01-04 and REF-18-01-04, Key Programme Special Fund (KSF) in XJTLU KSF-E-32 and KSF-E-21, and XJTLUConstruction of a Bioinformatics Platform for Precision Medicine: RDS10120180041.

ABSTRACT Human chromosome classification is essential to the clinical diagnosis of cytogenetical diseases such as genetic disorders and cancer. This process, however, is time-consuming and requires specialist knowledge. Considerable efforts have been made to automat the process. Recently, methods based on Convolutional Neural Networks achieved state-of-the-art results on the chromosome classification task. Many studies used karyotype images in performance evaluation, few studies have reported the results of human chromosome classification on microscopical images. This paper proposes a novel method to classify single chromosome images into one of 24 types. In the proposed method an extended ResNet was first devised to extract features of single chromosome images. A label feature vector was then extracted for each of 24 chromosome types based on a validation dataset. Hausdorff distance between feature vector of an input image and each of 24 label feature vectors were calculated, and the label feature vector that has minimum hausdorff distance to the feature vector of the input image was selected as the potential label of the input image. To finally allocate the single chromosomes from a same microscopical image into one of 24 types, a Label Redistribution strategy was used to shrink the label space and to increase the efficiency of chromosome classification. Experiments were implemented with 90,624 single chromosome images, 644 of which were randomly picked to form a testing set in advance. The classification accuracy on microscopical images using our proposed method achieved an accuracy of 94.72%.

INDEX TERMS Chromosome classification, ResNet, CNN, Hausdorff distance, microscopical images.

I. INTRODUCTION

Chromatin is the linear complex structure in the nucleus of interphase cells [1], which is composed of DNA (deoxyribonucleic acid), histones, non-histones and a small amount of RNA (Ribonucleic Acid). Chromosomes are the rods formed (thread-like structures) by the condensation of chromatin during mitosis or meiosis. It is invisible even under a microscope unless the DNA is in the metaphase stage of cell division. There are 46 chromosomes contained in each normal human cell nucleus (see (a) of figure 1), which can be classified into 22 pairs of autosomes as well as two gonosomes (see (b) of figure 1) [2]. By analyzing structural or numerical abnormalities of chromosomes [3], diseases such as genetic disorders, congenital defects and cancer, can be diagnosed in preliminary stage [4], [5]. These procedures are collectively known as karyotyping [6].

Distinguishing all single chromosomes in microscopical images demands specialist training and is very time-consuming. Computer-aided automatic approaches have gained much attention since the 1980s [7]–[9]. Automatic karyotyping generally consists of three steps: image preprocessing, segmentation and classification.

Traditional methods rely on manual extraction of features using Density Profile, which describes the geometrical distribution of centromere, long arm and short arm [6]. There are normally two strategies for locating the centromere: one relies on Media Axis Transform (MAT), which is more suitable

The associate editor coordinating the review of this manuscript and approving it for publication was Yudong Zhang.

for straight chromosomes [4], [10], and the other is based on Projection Vector (PV) methods which perform well on the bent chromosomes [11], [12]. It is not a trivial task for traditional methods to process a dataset consisting of both straight and curved chromosomes.

With the development of Deep Learning (DL) techniques, many DL architectures-based computer-aided methods have been proposed, and some of them have achieved state-of-the-art performance in the last decade. Deep Learning refers to abstract distinguishing information from input data via a model consisting of numerical layers [13]. Convolutional Neural Networks (CNN) is one class of DL model characterized by employing convolutional computation. Each convolutional kernel can be seen as a feature extractor. Several classical CNN models have achieved state-of-the-art performance on benchmark datasets. AlexNet achieved a milestone in employing Deep CNN on image classification in 2012 [14], [15]. ResNet [16] and Inception [17], [18] achieved layers beyond 50. Instance Segmentation strategy [19]–[21] and panoramic segmentation [22] achieved state-of-the-art performance in the object detection task.

Some researchers have studied the use of CNN structure in chromosomes classification [2], [23]. Similar to LeNet [24], AlexNet [14] and VggNet [25], these studies stack convolutional layer blocks followed by fully connected (FC) layers. They achieved classification accuracy of around 93%. Sharma *et al.* [26] proposed a Res-CRANN model which first extracts features via ResNet [16], then feeds those features to Long-Short Term Memory Networks (LSTM), which is then followed by an attention module. They achieved a classification accuracy of 91.94%. Qin *et al.* proposed a two-stage architecture of feature extraction and classification using fused features [27]. The highest accuracy obtained in the study on different cases was 99.2%.

Siamese architecture builds on the idea of classifying an input image by calculating the differences between a pair of images, which is the motivation for this research. Siamese architecture was proposed by Chopra *et al.* in 2005 for facial verification [28]. By minimizing a loss function via a unified architecture, a similarity metric between pairs of input data is developed. The value of the similarity metric between a genuine pair input will be much smaller than that of a fake pair input. This method was tested on the Purdue/AR face database and observed reasonable results. The idea of Siamese architecture was introduced to chromosome classification in a few studies. Somasundaram *et al.* [29] use a Probabilistic Neural Network (PNN) to calculate the ratio of chromosome arm length, and then compare the similarity distance. They tested their model on abnormal classification of 12 classes and obtained an accuracy of 97%. Swati *et al.* [30] proposed a Siamese network taking pairs of straightened chromosomes as input. They claimed to speed up the training steps as much as 83 times quicker. Their CNN consisted of two convolutional layers in addition to one FC layer.

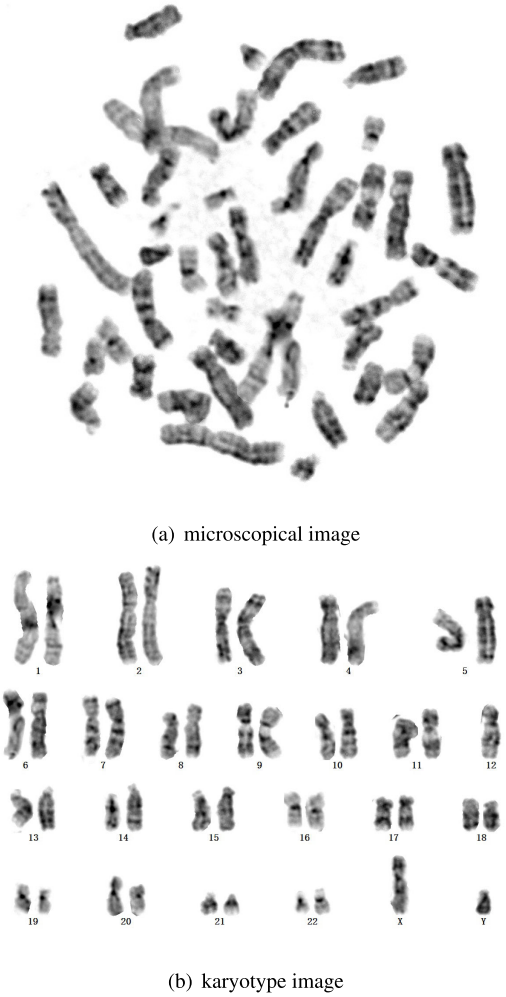

(a) microscopical image

(b) karyotype image

FIGURE 1. Microscopical and karyotype images: (a) is a microscopical image consisting of 46 individual chromosomes; (b) is a karyotype image also consisting of 46 individual chromosomes. Some chromosomes in (a) touch or overlap with each other, which could cause incomplete shape of chromosomes.

One of the difficulties with Siamese architecture is that the need for training data is doubled [28], [31], [32]. Moreover, it is much more challenging to classify single chromosome images extracted from microscopical images (SCMI) than single chromosome images extracted from karyotype images (SCKI), as the former is not always as regular as the latter, due to factors such as rotation, lack of shape, lower resolution, etc. Figure 1 shows their differences.

This paper proposes an extended ResNet model, combined with the Hausdorff Distance Calculation and a Label Redistribution strategy to classify single chromosomes into 24 classes. The rest of this paper is organized as follow: Section II explains the proposed methods in details. Section III describes the dataset, accuracy metric and comparison method. Section IV shows the results of the experiments which demonstrate the validity of the proposed methods. Finally, the conclusions of this paper are in given Section V.

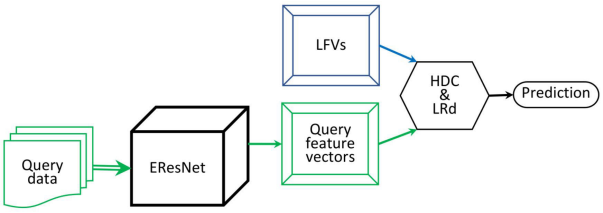

FIGURE 2. Overall diagram: Query data was classified by comparing their features (extracted from the CNN Model EResNet) with the matching Label Feature Vectors (LFV). This comparison procedure is the LRd strategy which consists of two round Hausdorff Distance Calculation (HDC).

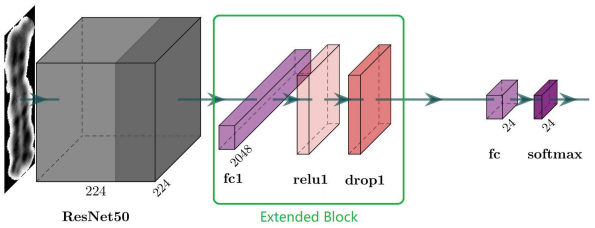

FIGURE 3. Structure of Extended ResNet: The output of ResNet50 is used as "features" and fed into the Extended Block, which is followed by a FC, and then a softmax classifier.

II. METHODOLOGY

This paper devises a CNN model, and uses its output for the calculation of Hausdorff distance [33], [34] between input images from "Query" set and Label Feature Vectors (LFV) from "Gallery" set. The idea behind Siamese architecture of comparing a pair of inputs to classify an image is utilized in this study. [35]. We use Gallery to denote images that will be used as a basis for judging categories, while Query refers to the set of images that will be labelled with the matched reference in the Gallery set.

The Label Feature Vectors derive from the Gallery set and will be used as feature vectors for distance comparing. They were generated by extracting features from the validation data and aggregating them into class 1 to 24. We propose a Label Redistribution (LRd) strategy based on the Hausdorff Distance Calculation, to calculate the distance between vectors from images in the Query set and the Label Feature Vectors, then the label corresponding to the minimal distance are mapped to the predicted label. LRd is a two round procedure to shrink label space via two round Hausdorff Distance Calculation which separates images together with labels into two sets after the first round calculation.

The overall diagram is shown in figure 2. Query feature vectors and Label Feature Vectors (LFV) are fed into the Hausdorff Distance Calculation (HDC) module, and then output for the label prediction.

A. EXTENDED ResNet MODEL

A classical CNN structure consists of convolutional layers, pooling layers and FC layers. A convolutional layer is essential in a CNN model. It is the operation of convolutional computation with a kernel. Each kernel can be seen as a feature extractor. A pooling layer (also known as downsampling layer) is sandwiched between continuous convolutional layers to compress the size of parameters and to reduce overfitting. In contrast to the convolutional and pooling layers, a FC layer maps the learned feature representation to the label space. FC layers are always employed in the last few layers. For convolutional and FC layer, activation function is required to enable them to be non-linear. Rectified Linear Unit (Relu) function $f(x) = max(0, x)$ is an activation function that is often used in CNN model. Here x is the output of a convolutional or FC layer, $f(x)$ is the output of Relu function.

Substantial studies employ ResNet [16] as their backbone [36], [37]. ResNet-50 indicates a ResNet structure composed of 50 layers, while ResNet-101 denotes a ResNet network consisting of 101 layers. ResNet adopts building block structure made up of a few stacked layers. In each block, the size of the output layer is the same as the size of the input layer.

In chromosome classification, CNN models based on ResNet have been attempted. Qin *et al.* adopted residual blocks for feature extraction in the proposed VarifocalNet [27]. Their method achieved an accuracy of 99.2% with *F1 score per-patient case*. Sharma *et al.* proposed a structure with residual module and attention strategy for a public dataset [26]. Their Top-1 classification accuracy achieved 91.94%.

Our proposed CNN model is based on the idea of residual block, which is the infrastructure of ResNet. Residual function $F(x) := H(x) - x$ is used to enable the connection between layers which are not directly connected, where x is the first input layer, $H(x)$ is the mapping of x, and $F(x)$ is the output of the stack. The output of ResNet-50 backbone is fed into the Extended Block, which consists of one unit consisting of a FC layer, a Relu layer, and a dropout layer in this sequence, as shown in figure 3. Another FC layer after the Extended Block. Its output is fed into a softmax classifier (24 classes). The input of the Extended Block will be used as "features" for Label Feature Vectors extraction in Section II-B and distance calculation in Section II-C. We name this model as Extended ResNet (EResNet).

Similar to Wen *et al.* [35], in this study we also combine the Softmax Loss L_s in equation 1 together with Center Loss L_c [35] in equation 2 as total loss L in equation 3 for the proposed EResNet model.

$$L_s = -\sum_{j=1}^{N} y_j log S_j \tag{1}$$

where N denotes the total number of classes. S_j is the jth value of the output vector from softmax layer, denoting the probability that this sample belongs to class j. y_j is 1 if this sample belongs to class j, and 0 otherwise.

Center Loss is defined as:

$$L_c = \sum_{j=1}^{m} \left\| x_j - c_{y_j} \right\|_2^2 \tag{2}$$

where m denotes the size of input, x_j is the feature vector of jth sample, and c_{y_j} is the feature center (a feature vector for a class, whose value can be seen as the mean of all feature vectors from this class) of y_jth class. $\|x_j - c_{y_j}\|_2^2$ denotes the squared Euclid distance between x_j and c_{y_j}. Center loss is used to make the distance between different classes larger, and makes classes more discriminative, therefore enhancing the classification accuracy.

$$L = L_s + \alpha L_c \tag{3}$$

where $\alpha \in (0, 1)$ is used for adjustings the weight of L_c, we set it to 0.5, the same value as used in Wen *et al.* [35].

The proposed Extended ResNet (EResNet) model is designed for Hausdorff Distance Calculation.

B. LABEL FEATURE VECTORS EXTRACTION

Before proceeding to chromosome classification, we extract feature vectors for all 24 label classes as Label Feature Vectors in advance. Specifically, we first extract features from input images in the validation dataset. Then we calculate the features of the 24 classes by obtaining the mean value of extracted feature vectors of all samples in the same class. We also add an amplifying coefficient factor γ to make the feature vector more distinguishable. The formula of calculating a Label Feature Vectors is shown below:

$$F_k = \gamma \frac{\sum_{j=1}^{M} f_k^j}{M} \quad k \in \{1, N_c\}, \quad \gamma \in [1, 1.5], \tag{4}$$

where F_k is the label feature vector of kth class,

M is the number of samples belonging to kth class,

N_c is the class number,

f_k^j is the feature vector of jth sample belonging to kth class,

γ is used to amplify the vector value to better distinguish those vectors. In this paper we empirically restrict γ to be a value between 1 to 1.5

C. HAUSDORFF DISTANCE CALCULATION AND CHROMOSOME CLASSIFICATION

Each image can be represented by a three dimension tensor. The metric to evaluate the similarity between two images is essential for enhancing classification accuracy in Siamese architecture. The Hausdorff distance [33], [34] compares the similarity between two images via difference of their element value (pixel). It is commonly used for comparing two sets of pixel values in computer vision task and is defined as:

$$H(A, B) = \max_{x \in A} \{\min_{y \in B} \{\|x, y\|\}\} \tag{5}$$

where $\|x, y\|$ is a normal distance such as Euclidean distance in equation 6. We use Hausdorff distance to evaluate the differences between two different input sets of an identical network model, then classify the input image by estimating if they belong to the same class. The input set with labelled class is named as Gallery set, and the one that is going to be labelled is named as Query set.

The Euclidean distance (L2 distance) and Cosine similarity distance between two feature vectors f^g and f^q are shown in equation 6 and 7 respectively.

Where for n dimension feature vector f^g, f^q,

$$q \in Q, \quad Q = \{q_1, q_2, \ldots, q_{bs}\}$$
$$g \in G, \quad G = \{g_1, g_2, \ldots, g_{24}\}$$

f_i^g is the value of ith element of feature vector f^g extracted from Label Feature Vectors of Gallery set.

f_i^q is the value of ith element of feature vector f^q extracted from the single image in Query set.

bs is the batch_size.

$$\|x, y\|_e = \sqrt{\sum_{i=1}^{n} (f_i^g - f_i^q)^2} \tag{6}$$

$$\|x, y\|_c = \frac{f^q \cdot f^g}{\|f^q\| \, \|f^g\|} = \frac{\sum_{i=1}^{n} f_i^q \times f_i^g}{\sqrt{\sum_{i=1}^{n} (f_i^q)^2} \times \sqrt{\sum_{i=1}^{n} (f_i^g)^2}} \tag{7}$$

Swati *et al.* [30] employ the Hausdorff L2 distance with Siamese architecture on chromosome classification, achieving a classification accuracy of around 85%. Their method compared differences between images from two sets. It requires extra input data used as Gallery set.

With the label feature vectors calculated in Section II-B, we directly use them as feature vectors of Gallery set. The feature vectors of Query set are extracted from input images in Query set as well.

We employ $\|x, y\|_c$ in equation 7 as the normal distance $\|x, y\|$ in equation 5 in this paper. The label g_{min} is selected as the predicted label of image with feature vector f^q, where $f^{g_{min}}$ is of the minimal distance $\|x, y\|_c$ from f^q.

D. LABEL REDISTRIBUTION

Once all distances between all f^g and f^q are calculated, and furthermore all f_{min}^g are selected, our next step is to identify the best match between query images and the 24 labels.

We proposed a Label Redistribution (LRd) strategy to shrink the solution space for increasing the possibility of correct prediction.

The procedure of LRd consists of two round Hausdorff Distance Calculation which is illustrated in figure 4:

- step 1: sort the distance list d^{first} in ascending order. The number of elements in list d^{first} is the same as batch size 46. Each element d_i in d^{first} is the distance between q_i and g_j, which is the minimal distance between q_i of Q and g_j of G. Note the predicted label of q_i is the label of g_j.
- step 2: given a sorted set d^{first} and a threshold number β whose value is between 1 and 45, d^{first} is divided into two sets d_{head}^{first} and d_{tail}^{first}, according to β. Specifically, we set β to 40 (and will explain the reason in Section IV-E), so the elements 41 to 46 together with their corresponding predicted labels form "tail" set, and the remained

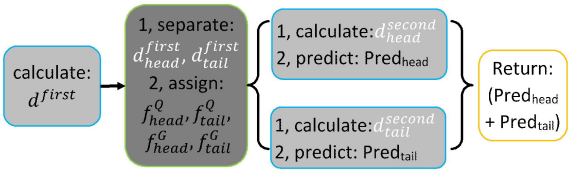

FIGURE 4. Label Redistribution.

40 elements as well as **remained labels** (some label of these 40 elements maybe picked out into "tail" set) form "head" set.

- step 3: the Hausdorff distance d^{second}_{head} were calculated from the separated "head" list set f^{Q}_{head} and f^{G}_{head}. Similarly, d^{second}_{tail} were calculated base on the "tail" lists f^{Q}_{tail} and f^{G}_{tail}. The classification results of d^{second}_{head} and d^{second}_{tail} were merged into the final prediction of input images from Query set.

Label redistribution is useful only when the potential correct samples (genuine pair) from Gallery set and Query set are still in the same list ("head" or "tail") after the separation in dark gray part of figure 4. Because the Query set was separated into two sets based on the value of distance, the Gallery set are also separated according to the prediction, which could be incorrect. Hence, once the sample and its correct label are separated into two set, this algorithm cannot be serviceable. For instance, if a sample from Query set with true label '3' is in "head" set, but wrongly predicted with label '4', and sample of Gallery with label '3' is picked out and put into the "tail" set, then this sample will not have the chance to be matched to the true label '3', hence it will not be correctly labelled with LRd.

III. EXPERIMENTS

All experiments were carried out on a Sugon workstation, with four NVIDIA 2080ti GPUs, two CPUs of Intel Xeon Silver 4110, and 64GB memory. The operating system is Ubuntu 18.04.03 LTS. The software framework is PyTorch 1.4 and the coding language is python 3.6.8.

A. DATASET

Each normal cell nucleus consists of 46 single chromosomes which can be classified into 24 classes. We name all these 46 chromosomes from the same cell nucleus as "one case". For abnormal cell, the total number of chromosomes may not be 46. Our experimental dataset is provided by a local company in Suzhou, China. It consists of 7 cases of Microscopical Images (MI) and 990 cases of Karyotype Images (KI). Each case was pre-processed in the same way before it is fed into the neural networks. Note that the shape of chromosome images from MI are not as regular as those from KI, due to overlap, touching, rotation, etc.. They are generally more difficult to be classified correctly.

For each case, all chromosomes were extracted manually and saved in ".jpg" format. The saved images were named with labels information, so the label can be obtained easily via file name.

Finally, we obtained 322 single chromosomes from 7 cases of MI. 7 cases among 990 cases of KI correspond to 7 cases of MI. From these 7 cases of KI, we also extracted 322 single chromosome images. From the rest of 983 (990-7) cases, we obtained 44,990 single chromosomes, which is 228 less than 45,218 ($45218 = (990 - 7) \times 46$). This is because we have 228 abnormal cases in our dataset. The 44,990 single chromosomes were flipped over to form another 44,990 cases of single chromosomes. Totally from 990 cases of KI we obtained 322+89980 single chromosomes. The ratio of validating is set to 10%. 80,286 images were randomly selected for training, the remaining 9694 were reserved for validating. There are "322 × 2" testing images as there are 322 images from MI corresponding to 322 from KI.

B. ACCURACY METRIC

Since the task of chromosome classification with 24 classes can be seen as a task with balanced sample data, we employed the evaluation method of accuracy shown in equation 8 rather than using precision, recall or F1-Score.

$$Acc = \frac{TP + TN}{TP + FP + TN + FN} \times 100\% \tag{8}$$

where TP is the number of correctly predicted chromosome images in the case, the number of wrong prediction is FP, both TN and FN are set to zero.

The average accuracy (Avg.) shown in equation 9 calculates the mean accuracy of all cases.

$$Avg = \frac{1}{N_c} \sum_{i=1}^{N_c} acc_i \tag{9}$$

where N_c is the number of cases, which is seven in this paper, acc_i is the accuracy of *ith* case which is calculated using equation 8.

C. COMPARISON METHOD

To compare the performance of our proposed methods, we also evaluated other two strategies of classification besides the proposed method, as follows:

- *Direct CNN classification (DCNN)*: uses a neural network model to classify input single images into 24 classes directly. *DCNN+MI* denotes Direct CNN classification and the Query set images are from Microscopical Images, while *DCNN+KI* denotes Direct CNN classification with the Query set images from Karyotype Images.
- *Classification based on feature vector match (FVM)*: In this experiment, feature vectors are extracted from single chromosome images separated from both karyotype images and original microscopical images. In this study, the set of single chromosome images from karyotype images is named as Gallery set (F^G), and the set of single chromosome images from microscopical images is named as Query set (F^Q). Hausdorff distance between images of F^G and images of F^Q is calculated,

and then used to classify the chromosome images. This is the same approach as traditional Siamese architecture based methods, which require pairs of image input (from Gallery set and Query set separately).

- *Classification based on feature vector match to label feature vectors (LFV)*: This experiment is similar to the previous experiment *FVM*, except that the Hausdorff distance is calculated between feature vectors of Query set (F^Q) images and 24 label feature vectors corresponds to 24 classes. The 24 label feature vectors were extracted from Gallery set F^G beforehand. This is the method we propose in this study. *LFV+MI* denotes that the Query set images are from Microscopical Images, while *LFV+KI* denotes that the Query set images are from Karyotype Images.

D. CNN MODELS

To assess the performance of the EResNet, we replace the EResNet with three popular CNN models: AlexNet, Vgg16, and ResNet50 [16] in the above three methods, and compare the performance of three methods and four CNN models on different Q and G image sets. AlexNet is the first milestone CNN model for image classification task [14]. It employed ReLU, Dropout, and Local Response Normalization in CNN for the first time. Vgg16 increased the depth to 16 weight layers and achieved the state-of-the-art performance with sequential connection on many applications [25].

IV. RESULTS AND DISCUSSION

Here we show the overall results of the three testing methods (*DCNN+MI*, *LFV+MI*, *DCNN+KI*, *LFV+KI* and *FVM*) and the four models, AlexNet, Vgg16, ResNet50 and EResNet on different Q and G image sets in table 1 and figure 5. From these results, we found that the proposed EResNet obtained the highest average accuracy using all of the testing methods except *DCNN+KI*, which is 0.62% lower than the result with AlexNet. The average from Microscopical Images (MI) is lower than the average from Karyotype Images (KI), because MI is more challenging. The average with *FVM* is highest, but it needs two image sets to compare their similarity, which is not as practical as the testing methods of *DCNN* and *LFV*. Figure 5 also illustrates that accuracy with LRd outperforms accuracy without LRd.

A. ACCURACY ON INDIVIDUAL CASES

We list the classification accuracy on all cases with testing methods *LFV+MI* and *LFV+KI* in the following table. Note that the accuracy of MI is higher than KI, as the β value we selected tends to get better performance on MI rather than KI:

The classification accuracy of case five is significantly lower than the other six cases. For Microscopical Images (MI), classification accuracy only achieved 82.61%, which is more than 10% lower than the other 6 cases. The listed wrongly predicted MI chromosomes from all cases are below:

The class 5, 14, 19, and 24 are wrongly predicted at least twice; we show all MI chromosomes of these classes in figure 6. From the images below we noticed seven of them (a, b, c, d, e, g, i) were rather tiny and contain an area that is much darker (marked with red box).

The testing method of *LFV+MI* compares the images from Query set with the Label Feature Vectors instead of images

TABLE 1. Overall average of three different testing methods with four models. The results in each row are obtained with the same model but may with different parameters, as we tried to find out the best performance of each method, by testing all the trained parameters and picking the highest results for each testing method. Finally, we identified the trained parameters of EResNet with highest LFV+MI 94.72% for subsequent experiments.

model	DCNN +MI (%)	LFV +MI (%)	DCNN +KI(%)	LFV +KI(%)	FVM (%)
AlexNet	89.75	91.30	92.55	93.17	93.17
Vgg16	89.13	91.62	91.61	94.10	95.34
ResNet50	83.23	86.65	86.65	90.06	87.27
EResNet	90.68	**94.72**	91.93	95.34	95.96

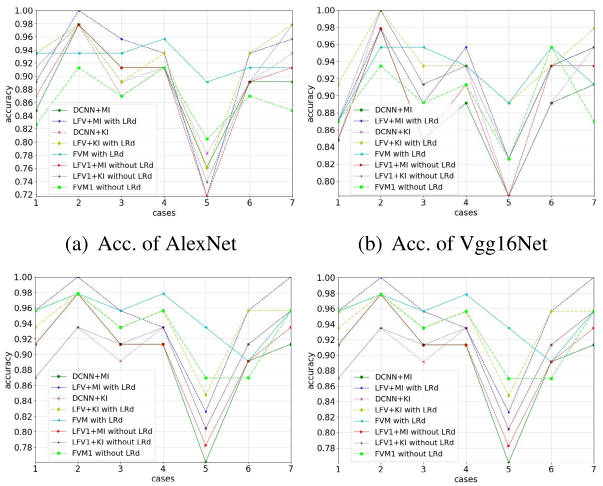

(a) Acc. of AlexNet (b) Acc. of Vgg16Net

(c) Acc. of ResNet50 (d) Acc. of EResNet

FIGURE 5. Accuracy of three different testing methods with four models of all cases.

TABLE 2. Classification accuracy on all seven cases:.

case	1	2	3	4	5	6	7	Avg.
LFV +MI (%)	95.65	100.0	95.65	93.48	*82.61*	95.65	100.0	94.72
LFV +KI(%)	93.48	97.83	93.48	95.65	84.78	95.65	95.65	93.79

TABLE 3. Wrong prediction of chromosomes of all seven cases: chromosome wrongly predicted three times: 19, 24; twice: 5, 14; once: 8, 11, 15, 14, 17.

case	wrong prediction
1	19-2 (21), 14-2(18)
2	None
3	24-1(17), 19-2(22)
4	24-1(8), 13-1(18), 5-2(23)
5	17-2(18),19-1(16),8-1(2),24-1(23),4-2(1),15-1(11),14-1(15), 11-1(14)
6	5-2(4), 18-2(20)
7	None

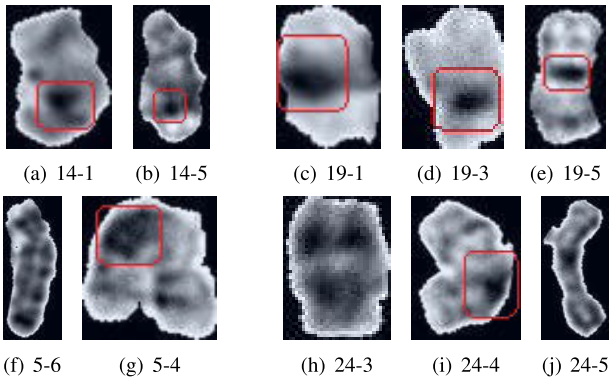

FIGURE 6. Chromosome images of wrongly predicted class 14 (a, b), 19 (c, d, e), 24 (h, i, j), 5 (f, g): the class number and case number are marked on the right to the series number (a) to (j). For instance: "(a) 14-1" indicates the chromosome belongs to class 14, and from case 1.

FIGURE 7. Chromosome images of original and the wrong prediction: (a) is from class 14, which was wrongly predicted as class 15; (d) belongs to class 19, and was wrongly predicted as class 16.

FIGURE 8. Correctly predicted chromosome images: the numbers in the caption are the classes of the corresponding images.

TABLE 4. Performance of different settings of Extended Block. The first digit 3, 2, 1, 0 in the model name denotes how many units (u) are in the Extended Block, in which each unit consists of a FC layer, a Relu layer, and a dropout layer. And the second digit 2, 1, 0 indicates which convolution layer (c) in the extended block from which the generated feature vector will be retained for LFV calculation. For instance, u2c1 indicates that there are two units in the Extended Block, and the output of the first convolutional layer is used for LFV calculation. The difference between 'u0c0' and ResNet50 is: 'u0c0' employs the joint loss in equation 3.

model	DCNN +MI (%)	LFV +MI (%)	DCNN +KI(%)	LFV +KI(%)	FVM (%)
u3c2	76.71	81.37	78.57	80.75	82.92
u3c1	90.68	93.79	91.61	94.41	95.96
u2c1	90.99	93.48	90.06	94.10	95.96
u1c1	90.68	93.17	90.68	93.79	95.34
u3c0	90.06	94.01	91.93	95.03	95.03
u2c0	89.44	94.10	91.30	95.03	95.34
u1c0	90.68	**94.72**	91.93	95.34	95.96
u0c0	90.37	94.10	91.30	95.34	95.96

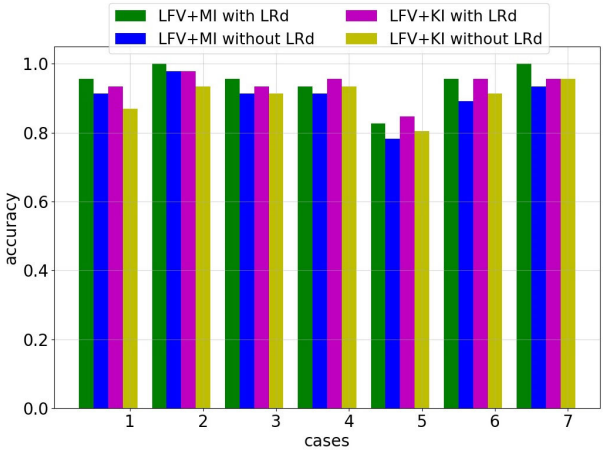

FIGURE 9. Accuracy of all cases with and without LRd: average of LFV+MI with LRd, LFV+MI without LRd, LFV+KI with LRd and LFV+KI without LRd are 94.72%, 90.37%, 93.79% and 90.37% respectively.

from Gallery set, then predicts the classification of input images (from Query set). We give the wrongly predicted original chromosome of class 14 and 19 from case five in figure 7 (a) and (d), together with their wrong prediction. Note that there are two images in all classes, except class 23 and 24, in which the sum of the chromosomes is two. The shape and dark area are very similar between the original and wrongly predicted images.

In Figure 8, we give some MI chromosomes which are not regular but were still correctly predicted by our proposed method.

B. SETTING OF EXTENDED BLOCK

Extended Block indicates the block structure extended after the output of ResNet50, shown as a green box in figure 3. To find the best Extended Block in figure 4, we tested different designs of Extended Block. We designed the Extended Block with different units, and used different layer output as features, then trained them for 300 epochs respectively. Figure 4 shows the results of the best accuracy of all designed models with three testing methods. We found the proposed EResNet with the Extended Block of one unit, and use the input of the Extended Block as features (u1c0) to achieve the highest classification accuracy of 94.72% on Microscopical Images.

C. LABEL REDISTRIBUTION STRATEGY

To verify the performance of the Label Redistribution (LRd), we show the accuracy both with and without it in Figure 9. We found that accuracy with LRd strategy surpasses the accuracy without LRd.

D. HAUSDORFF DISTANCE

Since Hausdorff distance is computed on a base distance metric, we compared two different base distance metrics, namely Euclid (Hausdorff+Euclid) and Cosine similarity distance (Hausdorff+Cosine). Figure 10 shows the accuracy of all seven cases of them on Microscopical Images.

In figure 10 (a), we notice that the overall accuracy with Hausdorff Cosine in both d^{first} (curve of first_cosine

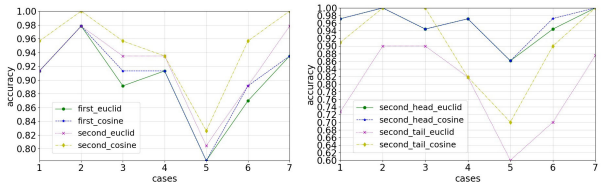

(a) accuracy of d^{first}, d^{second} (b) accuracy of d^{second}_{head}, d^{second}_{tail}

FIGURE 10. Accuracy of all cases with two different distances metric on MI. Average accuracy for four curves from top (green circle) to bottom (yellow diamond) in (a) is: [0.8975, 0.9037, 0.9193, 0.9472], while in (b) is [0.9561, 0.9601, 0.7886, 0.9039].

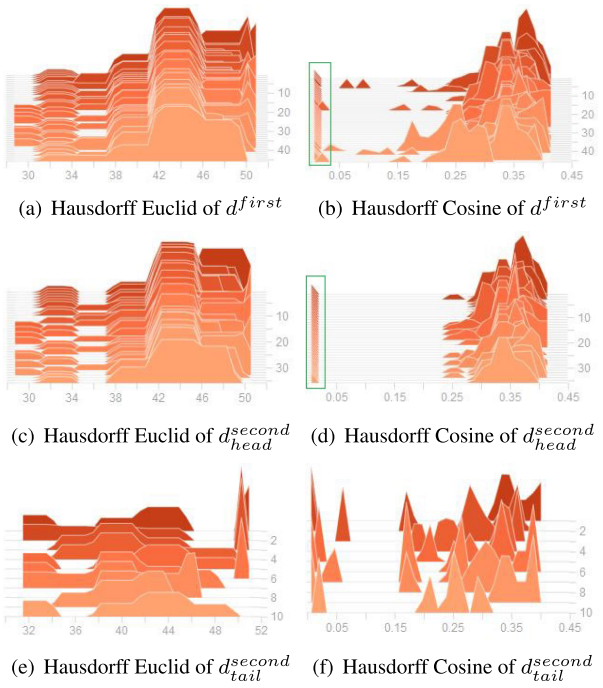

(a) Hausdorff Euclid of d^{first} (b) Hausdorff Cosine of d^{first}

(c) Hausdorff Euclid of d^{second}_{head} (d) Hausdorff Cosine of d^{second}_{head}

(e) Hausdorff Euclid of d^{second}_{tail} (f) Hausdorff Cosine of d^{second}_{tail}

FIGURE 11. Histograms of two distance metrics: *x*-axis are the 24 distance values between y and LFV, with each value corresponding to a class label; the minimal one will be picked out as predicted label; *y*-axis is from 1 to 46, which are the feature sequence in case three, stands for all 46 images from Query set; *z*-axis is the number of times a distance value appears. These histograms was smoothed for display, so the values of *x*-axis do not exactly correspond to the true distance value, but the whole tendency chart is reliable and more understandable.

with blue asterisk) and d^{second} (curve of second_cosine with yellow diamond) surpass the accuracy with Hausdorff Euclid (curve of first_euclid with green circle and curve of second_euclid with purple cross) respectively. We also find the accuracy with Hausdorff Cosine is higher than the accuracy with Hausdorff Euclid in figure 10 (b).

The difference of accuracy in case **three** is more distinguishable in figure 10 (a), and we show the distance value histogram figures of both distance metrics on case three in figure 11, including value from d^{first}, d^{second}_{head} and d^{second}_{tail}, to understand the reason visually. Note that the accuracy of d^{second} is not calculated directly by the correct prediction, but merged from the accuracy results of

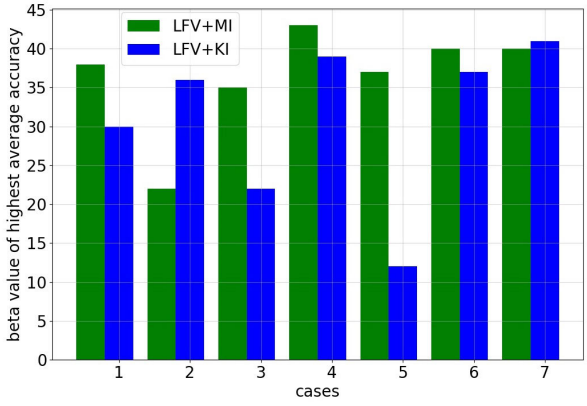

(a) best beta value in all cases

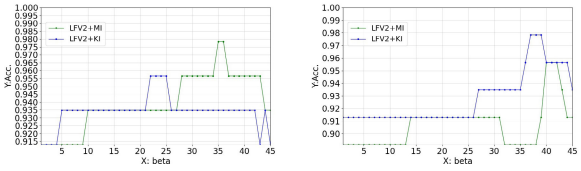

(b) Acc. with different beta value in case two (c) Acc. with different beta value in case five

FIGURE 12. Accuracy with different value of threshold β: best β value of cases 1 to 7 for *LFV+MI* is: [38, 22, 35, 43, 37, 40, 40], and for *LFV+KI* is: [30, 36, 22, 39, 12, 37, 41].

d^{second}_{head} and d^{second}_{tail} From the above figure, we found that the distance distribution of Hausdorff Cosine not only filters more values, but also distinguishes the minimal values on its left (marked with green rectangular box in (b) and (c)). Compared with (e), whose distance values almost distribute on a flat line for each feature, (f) spread only on about one third of classes. The accuracy also verified their performance with cyan line (2tail-Hausdorff_euclid) and red (2tail-Hausdorff_cosine) line in figure 10. So Hausdorff Cosine distance is indeed more distinguishable in our experiments and is more likely to predict the genuine minimal distance, which corresponds to the correct label.

E. THRESHOLD β

The value of threshold β contributes directly for the result of the proposed strategy. We checked the accuracy with different values of β, from minimal value one to maximal value 45 for all cases. Figure 12 (a) demonstrates the β value of highest accuracy of the seven cases. Figure 12 (b) and (c) shows accuracy on case **three** and **six** with different β values ranging from one to 45 respectively:

We found from figure 12 (a) that the accuracy of the first round is about 90%. The portion 0.90 indicates the threshold to 46 is $46 \times 0.9 = 40$. Figure 12 also indicates 40 always has the best accuracy, as the value of *y*-axis is the highest (or the second highest) when x is 40 on *x*-axis. We set threshold β to be 40 in this paper.

(a) 400 (b) 600

FIGURE 13. Differences between low and high resolution: (a) single chromosome from Karyotype Image (KI) with 400 bands; (b) KI with 600 bands.

V. CONCLUSION

In this study, we proposed a method for chromosome image classification, which is critical in computer aided automatic karyotyping. Our proposed method adopts EResNet and a LRd strategy which calculates Hausdorff Cosine distance with Label Feature Vectors. Our experiments demonstrated our method achieved an average accuracy of 94.72%, while only requiring one set images.

In the seven test cases, one of them showed poorer results. This abnormality motivated us to research further regarding this issue by using prior knowledge of chromosome band pattern to enhance the model's distinguishing ability.

Our work in this paper achieved a classification accuracy of 94.72%. For comparison, Swati *et al.* achieved accuracy of 85% with Siamese architecture on 1740 single chromosomes [30]. Sharma *et al.* achieved accuracy of 91.94% with proposed Res-CRANN [26]. Zhang *et al.* achieved accuracy of 92.5% with 10304 chromosomes [23]. Hu *et al.* achieved accuracy of 93.79% [2]. Lin *et al.* achieved accuracy of 95.98% based on Inception-ResNet, with 2990 single chromosomes [38]. Qin *et al.* reported the **F1-score per patient case** as 99.2% for classification tasks [27]. A better comparison with other methods would be to apply the methods on the same dataset. This however could not be achieved in this study, as either the datasets used in the other studies or the codes of the methods are not available to this study. This reduces the validity of this study to some extent.

In our experiments, we use low resolution chromosome images whose resolution is about 400 bands. Some other studies focus on much higher resolution images such as 600 bands. Figure 13 gives examples of chromosome images with 400 and 600 bands. Higher resolution images may help to improve the accuracy. However, more rigorous procedures and equipments are necessary to obtain those image data. In this study, only low resolution images are available.

Our proposed EResNet focus on the linear extension of ResNet 50 by adding fully connected layers, it may lack the ability of extracting special features efficiently. The LVFs were extracted via validation dataset, as a consequent, LVFs are restricted by the used validation dataset, which influence the classification performance of the proposed method. The selection of the value β also impacts the model ability of shrinking solution space, which may impact the chromosome classification accuracy. The performance of this research could be enhanced by replacing ResNet50 backbone with others, such as ResNeXt [39] or DPN [40].

Our future work will also include research on the public datasets such as BioImLab [26], and research on applications of the proposed method in other medical fields. In this study the proposed method was applied on single chromosomes obtained manually from microscopic chromosome images. In our next step we will combine our chromosome segmentation and classification, and classify chromosomes with the proposed method directly on individual chromosomes obtained by the segmentation algorithm on microscopic images.

REFERENCES

[1] M. Park, "What is a chromosome?" *J. Pathol.*, vol. 163, no. 3, pp. 185–189, 1991.
[2] X. Hu, W. Yi, L. Jiang, S. Wu, Y. Zhang, J. Du, T. Ma, T. Wang, and X. Wu, "Classification of metaphase chromosomes using deep convolutional neural network," *J. Comput. Biol.*, vol. 26, no. 5, pp. 473–484, May 2019.
[3] B. B. Ganguly, D. Banerjee, and M. B. Agarwal, "Impact of chromosome alterations, genetic mutations and clonal hematopoiesis of indeterminate potential (CHIP) on the classification and risk stratification of MDS," *Blood Cells, Molecules, Diseases*, vol. 69, pp. 90–100, Mar. 2018.
[4] X. Wang, "Development of a computer-aided chromosome analysis system to assist cancer diagnosis," Ph.D. dissertation, Graduate College, Univ. Oklahoma, Norman, OK, USA, 2008.
[5] B. Feng, D. C. Samuels, W. Hoskins, Y. Guo, Y. Zhang, J. Tang, and Z. Meng, "Down syndrome prediction/screening model based on deep learning and illumina genotyping array," in *Proc. IEEE Int. Conf. Bioinf. Biomed. (BIBM)*, Kansas City, MO, USA, , Nov. 2017, pp. 347–352.
[6] F. Abid and L. Hamami, "A survey of neural network based automated systems for human chromosome classification," *Artif. Intell. Rev.*, vol. 49, no. 1, pp. 41–56, Jan. 2018.
[7] B. Lerner, "Toward a completely automatic neural-network-based human chromosome analysis," *IEEE Trans. Syst., Man Cybern., B (Cybern.)*, vol. 28, no. 4, pp. 544–552, Aug. 1998.
[8] M. Popescu, P. Gader, J. Keller, C. Klein, J. Stanley, and C. Caldwell, "Automatic karyotyping of metaphase cells with overlapping chromosomes," *Comput. Biol. Med.*, vol. 29, no. 1, pp. 61–82, Jan. 1999.
[9] M. Moradi and S. K. Setarehdan, "New features for automatic classification of human chromosomes: A feasibility study," *Pattern Recognit. Lett.*, vol. 27, no. 1, pp. 19–28, Jan. 2006.
[10] B. Lerner, H. Guterman, I. Dinstein, and Y. Romem, "Feature selection and learning curves of a multilayer perceptron chromosome classifier," in *Proc. 12th IAPR Int. Conf. Pattern Recognit.*, vol. 3, Oct. 1994, p. 497.
[11] N. Madian, K. B. Jayanthi, and S. Suresh, "Contour based segmentation of chromosomes in G-band metaphase images," in *Proc. IEEE Global Conf. Signal Inf. Process. (GlobalSIP)*, Dec. 2015, pp. 943–947.
[12] N. Madian, K. B. Jayanthi, and S. Suresh, "Analysis of human chromosome images: Application towards an automated chromosome classification," *Int. J. Imag. Syst. Technol.*, vol. 28, no. 4, pp. 235–245, Dec. 2018.
[13] Y. LeCun, Y. Bengio, and G. Hinton, "Deep learning," *Nature*, vol. 521, pp. 436–444, May 2015.
[14] A. Krizhevsky, I. Sutskever, and G. Hinton, "ImageNet classification with deep convolutional neural networks," in *Proc. 25th Int. Conf. Neural Inf. Process. Syst. (NIPS)*, vol. 1. Lake Tahoe, NV, USA, Dec. 2012, pp. 1097–1105.
[15] M. D. Zeiler and R. Fergus, "Visualizing and understanding convolutional networks," in *Proc. Eur. Conf. Comput. Vis.*, Zurich, Switzerland, 2014, pp. 818–833.
[16] K. He, X. Zhang, S. Ren, and J. Sun, "Deep residual learning for image recognition," in *Proc. IEEE Conf. Comput. Vis. Pattern Recognit. (CVPR)*, Las Vegas, NV, USA, Jun. 2016, pp. 770–778.

[17] C. Szegedy, W. Liu, Y. Jia, P. Sermanet, S. Reed, D. Anguelov, D. Erhan, V. Vanhoucke, and A. Rabinovich, "Going deeper with convolutions," in *Proc. IEEE Conf. Comput. Vis. Pattern Recognit. (CVPR)*, Boston, MA, USA, Jun. 2015, pp. 1–9.
[18] C. Szegedy, S. Ioffe, V. Vanhoucke, and A. Alemi, "Inception-v4, inception-resnet and the impact of residual connections on learning," in *Proc. 31st AAAI Conf. Artif. Intell.*, Feb. 2017, pp. 4278–4284.
[19] K. He, G. Gkioxari, P. Dollár, and R. Girshick, "Mask R-CNN," in *Proc. IEEE ICCV*, Venice, Italy, Dec. 2017, pp. 2980–2988.
[20] R. Hu, P. Dollar, K. He, T. Darrell, and R. Girshick, "Learning to segment every thing," in *Proc. IEEE/CVF Conf. Comput. Vis. Pattern Recognit.*, Jun. 2018, pp. 4233–4241.
[21] Y. Li, H. Qi, J. Dai, X. Ji, and Y. Wei, "Fully convolutional instance-aware semantic segmentation," in *Proc. IEEE Conf. Comput. Vis. Pattern Recognit. (CVPR)*, Jul. 2017, pp. 4438–4446.
[22] A. Kirillov, R. Girshick, K. He, and P. Dollar, "Panoptic feature pyramid networks," in *Proc. IEEE/CVF Conf. Comput. Vis. Pattern Recognit. (CVPR)*, Long Beach, CA, USA, Jun. 2019, pp. 6399–6408.
[23] W. Zhang, S. Song, T. Bai, Y. Zhao, F. Ma, J. Su, and L. Yu, "Chromosome classification with convolutional neural network based deep learning," in *Proc. 11th Int. Congr. Image Signal Process., Biomed. Eng. Informat. (CISP-BMEI)*, Beijing, China, Oct. 2018, pp. 1–5.
[24] Y. LeCun, L. Bottou, Y. Bengio, and P. Haffner, "Gradient-based learning applied to document recognition," *Proc. IEEE*, vol. 86, no. 11, pp. 2278–2324, Nov. 1998.
[25] K. Simonyan and A. Zisserman, "Very deep convolutional networks for large-scale image recognition," in *Proc. 3rd Int. Conf. Learn. Represent.*, 2014. [Online]. Available: http://arxiv.org/abs/1409.1556
[26] M. S. Sharma and L. Vig, "Automatic chromosome classification using deep attention based sequence learning of chromosome bands," in *Proc. Int. Joint Conf. Neural Netw. (IJCNN)*, Rio de Janeiro, Brazil, Jul. 2018, pp. 1–8.
[27] Y. Qin, J. Wen, H. Zheng, X. Huang, J. Yang, N. Song, Y.-M. Zhu, L. Wu, and G.-Z. Yang, "Varifocal-net: A chromosome classification approach using deep convolutional networks," *IEEE Trans. Med. Imag.*, vol. 38, no. 11, pp. 2569–2581, Nov. 2019.
[28] S. Chopra, R. Hadsell, and Y. LeCun, "Learning a similarity metric discriminatively, with application to face verification," in *Proc. IEEE Comput. Soc. Conf. Comput. Vis. Pattern Recognit. (CVPR)*, vol. 1. San Diego, CA, USA, Jun. 2005, pp. 539–546.
[29] D. Somasundaram, N. Kumaresan, V. Subramanian, and S. Sacikala, "Structural similarity and probabilistic neural network based human g-band chromosomes classification," *Int. J. Hum. Genet.*, vol. 18, no. 3, pp. 228–237, Seq 2018.
[30] S. Jindal, G. Gupta, M. Yadav, M. Sharma, and L. Vig, "Siamese networks for chromosome classification," in *Proc. IEEE Int. Conf. Comput. Vis. Workshops (ICCVW)*, Venice, Italy, Oct. 2017, pp. 72–81.
[31] J. Bromley, J. W. Bentz, L. Bottou, I. Guyon, Y. Lecun, C. Moore, E. Säckinger, and R. Shah, "Signature verification using a 'siamese' time delay neural network," *Int. J. Pattern Recognit. Artif. Intell.*, vol. 7, no. 4, pp. 669–688, 1993.
[32] D. Yi, Z. Lei, S. Liao, and S. Z. Li, "Deep metric learning for person re-identification," in *Proc. 22nd Int. Conf. Pattern Recognit.*, Stockholm, Sweden, Aug. 2014, pp. 34–39.
[33] D. P. Huttenlocher, G. A. Klanderman, and W. J. Rucklidge, "Comparing images using the hausdorff distance," *IEEE Trans. Pattern Anal. Mach. Intell.*, vol. 15, no. 9, pp. 850–863, Sep. 1993.
[34] A. A. Taha and A. Hanbury, "An efficient algorithm for calculating the exact hausdorff distance," *IEEE Trans. Pattern Anal. Mach. Intell.*, vol. 37, no. 11, pp. 2153–2163, Nov. 2015.
[35] Y. Wen, K. Zhang, Z. Li, and Y. Qiao, "A discriminative feature learning approach for deep face recognition," in *Proc. Eur. Conf. Comput. Vis.*, Amsterdam, Netherlands, 2016, pp. 499–515.
[36] S. Ren, K. He, R. Girshick, and J. Sun, "Faster R-CNN: Towards real-time object detection with region proposal networks," *IEEE Trans. Pattern Anal. Mach. Intell.*, vol. 39, no. 6, pp. 1137–1149, Jun. 2017.
[37] Z. Huang, L. Huang, Y. Gong, C. Huang, and X. Wang, "Mask scoring R-CNN," in *Proc. IEEE/CVF Conf. Comput. Vis. Pattern Recognit. (CVPR)*, Jun. 2019, pp. 6402–6411.
[38] C. Lin, G. Zhao, Z. Yang, A. Yin, X. Wang, L. Guo, H. Chen, Z. Ma, L. Zhao, H. Luo, T. Wang, B. Ding, X. Pang, and Q. Chen, "CIR-net: Automatic classification of human chromosome based on inception-resnet architecture," *IEEE/ACM Trans. Comput. Biol. Bioinf.*, early access, Jun. 18, 2020, doi: 10.1109/TCBB.2020.3003445.
[39] S. Xie, R. Girshick, P. Dollar, Z. Tu, and K. He, "Aggregated residual transformations for deep neural networks," in *Proc. IEEE Conf. Comput. Vis. Pattern Recognit. (CVPR)*, Jul. 2017, pp. 5987–5995.
[40] Y. Chen, J. Li, H. Xiao, X. Jin, S. Yan, and J. Feng, "Dual path networks," in *Proc. Adv. Neural Inf. Process. Syst. (NIPS)*, vol. 30, 2017, pp. 4467–4475.

CHENGYU WANG was born in China, in 1982. He received the master's degree in software engineering from Southeast University, Nanjing, Jiangsu, China, in 2009. He is currently pursuing the Ph.D. degree with the University of Liverpool, Suzhou. He has published two conference papers in last year. His research interests include medical image process with deep learning strategy, especially human-chromosome karyotype segmentation and classification.

LIMIN YU (Member, IEEE) received the B.Eng. degree in telecommunications engineering and the M.Sc. degree in radio physics/underwater acoustic communications from Xiamen University, China, and the Ph.D. degree in telecommunications engineering from The University of Adelaide, Australia.

She was with ZTE Telecommunication Company Ltd., Shenzhen, China, as a Software Engineer. She was also with the University of South Australia and The University of Adelaide, as a Research Fellow and a Research Associate. She is currently an Associate Professor with the Electrical and Electronic Engineering Department, Xi'an Jiaotong-Liverpool University, Suzhou, China. Her research interests include sonar detection, wavelet analysis, filter bank design, broadband system design, high-mobility wireless local area networks, sensor networks, and medical image analysis.

XU (JUDY) ZHU (Senior Member, IEEE) received the B.Eng. degree (Hons.) from the Huazhong University of Science and Technology, Wuhan, China, in 1999, and the Ph.D. degree from The Hong Kong University of Science and Technology, Hong Kong, in 2003.

She has over 180 peer-reviewed publications in leading international journals and conference proceedings on communications and signal processing. She received the Research Income of over £1.5 M from various funding bodies, such as EPSRC, EU, TSB, Industry, and so on. Her research interests include MIMO, OFDM, equalization, millimetre-wave transmission, blind source separation, cooperative communications, cognitive radio, cross-layer optimization, smart grid communications, green communications, and so on.

Dr. Zhu is a member of IET. She received the Best Paper Award from the IEEE Globecom in 2019. She has been actively engaged in organising international conferences and workshops as the chair, such as the Publicity Chair of the IEEE IUCC in 2015, and the Symposium Chair of the IEEE ICC in 2016 and 2019. She served as the Editor for the IEEE TRANSACTIONS ON WIRELESS COMMUNICATIONS and a Guest Editor for Special Issues for various journals, such as *Electronics*.

JIONGLONG SU received the Ph.D. degree in statistics, Warwick, and the Ph.D. degree in automatic control and systems engineering, Sheffield.

He was with the University of Warwick, University College London, and Nazarbayev University, where he was also the Maths Head. He is currently the Deputy Dean of the School of Artificial Intelligence and Advanced Computing, Xi'an Jiaotong-Liverpool University Entrepreneur College, Taicang. His research interests include bioinformatics, artificial intelligence, and medical image processing.

FEI MA received the B.Sc. and M.Sc. degrees of computational mathematics from Xiamen University, China, and the Ph.D. degree in applied mathematics from Flinders University, Australia.

He was an Analyst with Symbion, Australia, a Research Associate and a Lecturer with Flinders University, and a Software Engineer with Kingdee Company Ltd., Shenzhen. He is currently a Senior Associate Professor with the Applied Mathematics Department, Xi'an Jiaotong-Liverpool University, Suzhou, China. His research interests include medical and biomedical image analysis, including computer aided breast cancer diagnosis with mammogram, cell image and chromosome image analysis, big data analytics, AGV scheduling and routing, and nonnegative matrices.